

Wide-Band Directional Cavity Antenna with Low Scanning Loss for WLAN

Somanatha Swapna^{1, *}, Gudur S. Karthikeya², Shibani K. Koul¹, and Ananjan Basu¹

Abstract—In this paper, a wide-band cavity antenna with low scanning loss for 20% antenna bandwidth as well as having a wide 20% 1-dB gain bandwidth over the antenna beam scanning angle is proposed. The antenna operates in the 5 GHz band of IEEE 802.11 ac wireless local area network (WLAN) applications. A beam scanning of 20° is demonstrated by varying the height of a slider within the antenna cavity. The broadside peak gain of 9.6 dBi is maintained for 20% of the antenna bandwidth with a gain reduction of only 0.3 dB throughout its operating frequency range. Besides, the scanning loss suffered by the antenna when scanning from the broadside to the maximum scanned angle is only 0.8 dB. The proposed scan performance is verified for a single element antenna and a two-element antenna array.

1. INTRODUCTION

The evolution of various wireless communication systems has given rise to a necessity to design wide-band antennas with high-gain and stable radiation patterns across the operating band for base stations to receive and transmit signals. The IEEE 802.11 ac WLAN has the bandwidth necessary to meet excess demand and high data rates [1]. Now, adequate angular coverage is necessary making beam scanning an important feature of the antenna systems. There are two scanning losses associated with antennas: first, the fall in gain when the beam is scanned from broadside to the scanned angle and second, the fall in gain when the frequency of the antenna is varied from the resonant frequency within the bandwidth. In this paper, we propose a design that reduces these scanning losses to the lowest possible level. It is important in antenna designs to reduce these losses so that the signal strength is maintained throughout the desired range.

Conventional beam scanning methods can be broadly classified into electronic and mechanical beam scanning. In electronic scanning, a phased array enables fast and continuous beam scanning within certain angular space. But they require phase shifters to control the phase of each element which in turn is limited by the bandwidth [2]. When an array is scanned with fixed units of phase shifters, the main beam position changes with frequency. The bandwidth of the phased array antenna is limited by the phase shifters [3]. The scanning of the phased array is accomplished by using diode or ferrite phase shifters. [4] has reported a scanning loss of 2.26 dB for a 45° scan. So, the coverage of the phased array antennas with pattern integrity is limited. Instead of using phase shifters to steer the radiation, pin diodes [5], varactor diodes [6], RF-MEMS switches [7] can also be used to steer the beam. But the extra bias lines needed for their operation make the antenna design more complex. Despite having high-speed beam scanning, these antennas suffer from design complexity, high fabrication cost, and high losses resulting in low efficiency. Conventional mechanical beam scanning antennas consist of moving reflector antennas [8] that are massive in size. An alternate solution to reduce the cost and weight of the antennas is to use transmitarray [9] or reflectarray design [10]. The lenses are flexible and offer some

Received 16 January 2022, Accepted 23 February 2022, Scheduled 2 March 2022

* Corresponding author: Somanatha Pai Swapna (s.swapna.pai@gmail.com).

¹ Centre for Applied Research in Electronics (CARE), Indian Institute of Technology Delhi, India. ² Centre for Antennas and Radio Frequency Systems, Ramaiah Institute of Technology, Bangalore, India.

flexibility to the antenna design [11]. However, its performance declines for wide scan angles due to high scanning losses, and the lens makes the antenna bulky. In [12], a waveguide antenna is presented where the beam scanning is achieved by rotating a dielectric slab. In [13], beam steering is obtained by independently rotating the metasurfaces around the antenna axis. However, for the antennas mentioned in the literature, the bandwidth for which the beam scanning is sustained is very limited and for the most part varies within the bandwidth.

The proposed design in this paper uses 3-D printing technology for antenna fabrication over the traditional photolithographic process. This is considering the fact that the proposed antenna has a 3-D structure and not a planar one. 3-D printing is a sought-after technology today as it allows rapid development of robust, compact, and light-weight objects at an affordable cost [14]. This technology is now widely used for antenna fabrication as well. 3-D printing allows more complex antenna designs like intricately shaped substrates as in [15], the inhomogeneous substrate as reported in [16], or using multiple materials in antenna designs as reported in [17]. After 3-D printing, different metallization processes like electroless plating [18] and conductive paints [19] are used to create the conductive parts of the antenna. In this paper, the metallization of the 3-D printed substrate is done by pasting copper tapes at the necessary locations. This is a very low-cost method compared to other metallization processes adopted in the literature.

The impact on system performance due to the antenna tilt in GSM is examined in [20]. It is seen that to enhance angular coverage on the ground, the base station antenna is tilted, mechanically. A power coupler comprising an electromechanical phase shifter that can adjust phase by the relative motion of components is claimed in [21]. This technique is **widely being used commercially** in many mobile systems. Even though it applies to wide frequency bands, this type of phase control by the phase shifter circuits results in higher losses and needs extra circuitry as well. Traditionally, the beam tilt of base station antennas is controlled by ensuring that the antennas have sufficient tilt to reach the intended users. The antennas are tilted downwards physically along with required phase shifts [22]. But these are low-frequency Global System for Mobile Communications (GSM) band antennas where such techniques provide expected beam tilts. The proposed beam tilting technique is a much simpler solution for high-frequency antenna beam tilts. In this method, we shift the height of a slider inside an antenna cavity, while avoiding the use of any phase shifters throughout the design. This technique is much more robust than the standard antennas that are connected to feed networks and physically supporting networks.

In contrast to previous works, where researchers have proposed numerous wide-band antennas with omnidirectional radiations [23, 24], the proposed design is a wide-band unidirectional antenna with scanning loss of only 0.3 dB throughout the bandwidth. In previous works like [25], a wideband antenna with directional radiation, in just 1 GHz of antenna bandwidth, the antenna suffers from 1.1 dB scanning loss. The antenna design also lacks the beam scanning ability. [26] proposed a wideband cavity antenna with a large ground plane where the gain varies from 0 to 6.8 dB within a 28% fractional bandwidth at 2.3 GHz. The antenna has wide beamwidth making it poorly directional. The proposed antenna has a large ground plane and a unidirectional pattern that gives the opportunity to mount back-end electronics. When antennas are integrated with other back-end electronic devices, its performance is significantly affected by the ground plane structure [27]. This occurs due to the field coupling between the antenna and the device ground plane. In such instances, an electrically large ground plane would act as an isolating shield against the potential interference from the active electronic circuitry. The proximity to a conducting ground plane makes the bandwidth of a patch antenna deteriorate [28]. To increase the bandwidth of the antenna, we can increase the height or reduce the dielectric constant of the substrate. However as mentioned in [29], this approach can be used for $h < 0.02\lambda$ only. [30] reports that when a rectangular plate is placed over a ground plane, as the height of the plate is varied from 0.125λ to 0.25λ there is a reduction of Q factor by a factor of 2. In the proposed design, the height of the antenna is fixed at 0.1λ making it an electrically compact design, and at the same time the antenna is wideband in nature. Besides, the proposed design, having the benefit of being unidirectional, allows for easy integration with ceiling mounted back end electronics without any influence on the performance of the antenna. The proposed antenna scans the beam from broadside to 20° with scanning loss of only 0.8 dB. So the proposed design is also able to maintain wide 20% 1-dB gain bandwidth throughout its scanning range. Phase shifters used in conventional array designs result in high insertion loss. The

absence of any phase shifters or active devices in the proposed design consequently eliminates any insertion loss associated with the antenna.

2. CAVITY ANTENNA DESIGN

2.1. Narrow-Band Cavity Antenna

Consider a conventional patch antenna. The bandwidth of a patch antenna can be increased by increasing the thickness of the substrate or by reducing the dielectric constant of the substrate [29]. To achieve finer characteristics than a conventional patch, a cavity antenna as shown in Fig. 1 is considered. The chosen substrate for the antenna design is polylactic acid (PLA) with $\epsilon_r = 2.58$ and $\tan \delta = 0.015$. PLA is a user-friendly thermoplastic for 3D printing performed by the Fused Deposition Modelling (FDM) method. The height of the cavity antenna is 5 mm. Here, from the 5 mm PLA block, 4 mm of the substrate is removed to make the cavity. Now, the cavity consists of air as the substrate with a dielectric constant of 1. A 0.5 mm thickness of PLA substrate is used at the top and bottom to make the cavity antenna as shown in Fig. 1(b) as walls of the cavity antenna. A 4 mm thickness was considered at the sides of the cavity walls to adequately support the antenna structure. This lateral support is necessary and can be obtained only through 3-D printing as it will be attached firmly to the other sides as well which is only 0.5 mm in thickness. Using other dielectric substrates sections to build the cavity cannot ensure the stability obtained through the 3-D printing method. Consequently, 3-D printing using PLA was chosen even though the PLA substrate has a relatively high loss tangent, which could affect the radiation efficiency of the antenna.

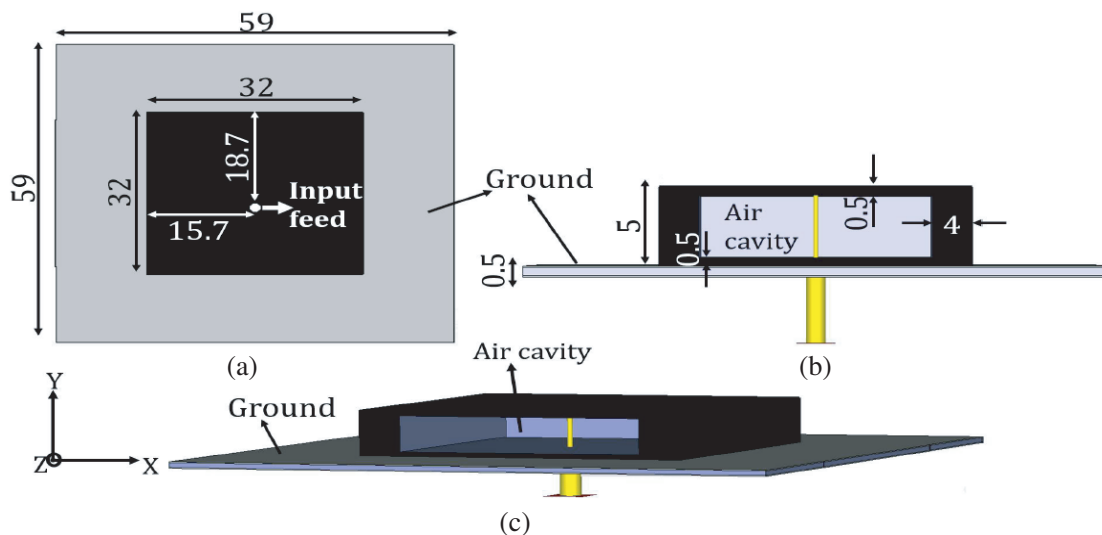


Figure 1. Schematic of narrow-band cavity antenna. (a) Top view. (b) Side view. (c) Isometric view (Unit: mm).

The cavity antenna has a square structure with its edge lengths at 32 mm (0.6λ). The bottom of the cavity antenna body consists of a 59 mm ground plane. The input port is connected to the top layer of the antenna through a coaxial feed. The return loss of the cavity antenna is depicted in Fig. 2(a) with the bandwidth of the antenna from 5.58 GHz to 6 GHz. The radiation pattern at 5.8 GHz is shown in Fig. 2(b). The gain of the antenna at the resonant frequency of 5.8 GHz is 5.8 dBi.

2.2. Wide-Band Cavity Antenna

The narrow-band cavity antenna is further modified to realize a wide-band cavity antenna. The schematic view of the wide-band cavity antenna is shown in Fig. 3. To increase the impedance bandwidth, various slots are introduced at specific positions as shown in Fig. 3(a). The narrow band

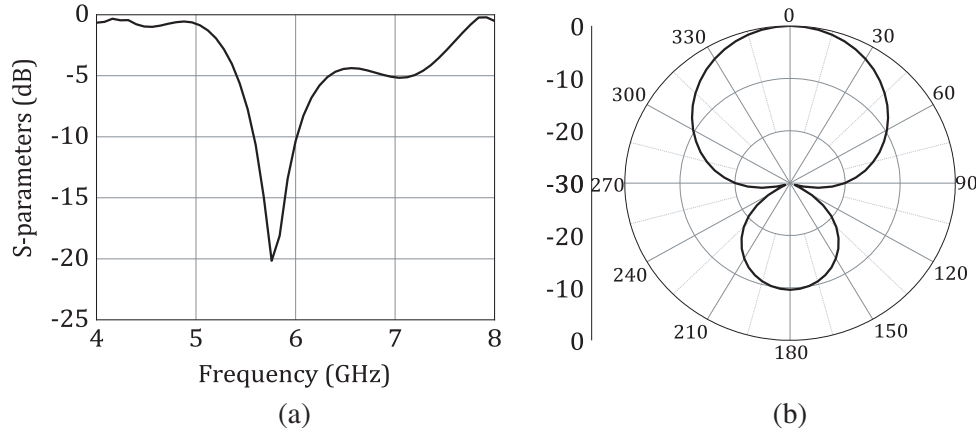


Figure 2. (a) Return loss of the narrow-band cavity antenna. (b) Radiation Pattern of the narrow-band cavity antenna at 5.8 GHz.

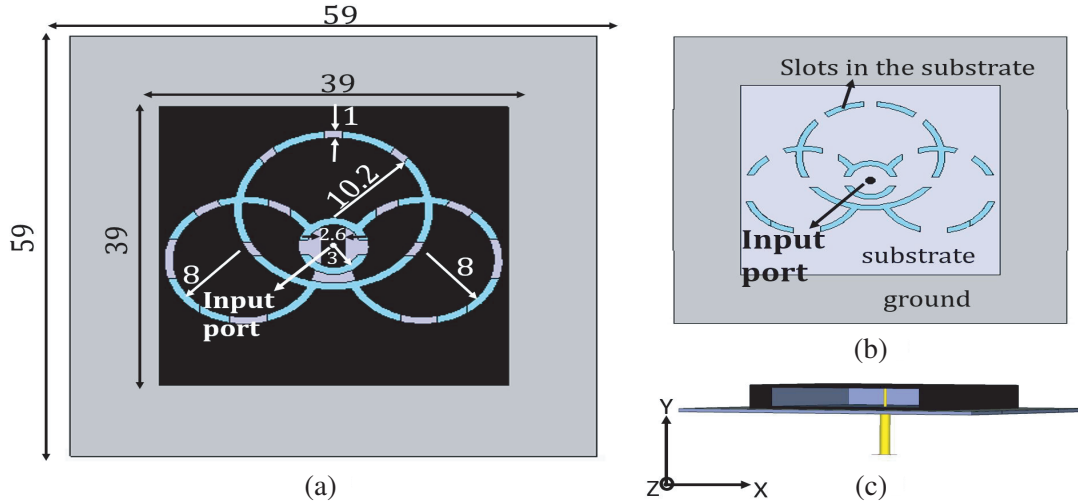


Figure 3. Schematic of wide-band cavity antenna. (a) Top view. (b) Top view of the substrate. (c) Isometric view.

cavity antenna has a single opening in the cavity that aids in radiation. This is seen in Fig. 1(b) where the front part of the cavity is removed. To increase the bandwidth, slots were made in the metal and substrate, which increased the openings through which the radiation will occur. This increased energy loss reduces the quality factor of the cavity increasing the bandwidth of the antenna. At first, the slots are introduced at the top metal part of the antenna with a slot width of 1 mm throughout. Fig. 5(a) shows the return-loss variation of the antenna with the introduction of each circular slot. Slot 1 indicates the circle with a radius of 10.2 mm and a 1 mm slot towards the edge of the circle. Slot 2 is the circle at the center with a radius of 3 mm. Finally, two circles with a radius of 8 mm are introduced at two sides, referred to as slot 3. The slots introduced in the metal layer are sufficient for a wide-band cavity antenna. However, it was observed that the slider that has to be placed inside the antenna cavity causes severe detuning of the antenna. To overcome this detuning effect, just like the slots in the metal layer similar slots were created on the substrate as well. To ensure continuity in the substrate, some segments of the slots were closed strategically such that it does not affect the results considerably. The slots also increase the electrical length of the antenna. The surface current distributions of the cavity antenna without and with various slots are shown in Figs. 4(a)–(d). The slots force the surface currents to meander, artificially increasing the electrical length of the antenna

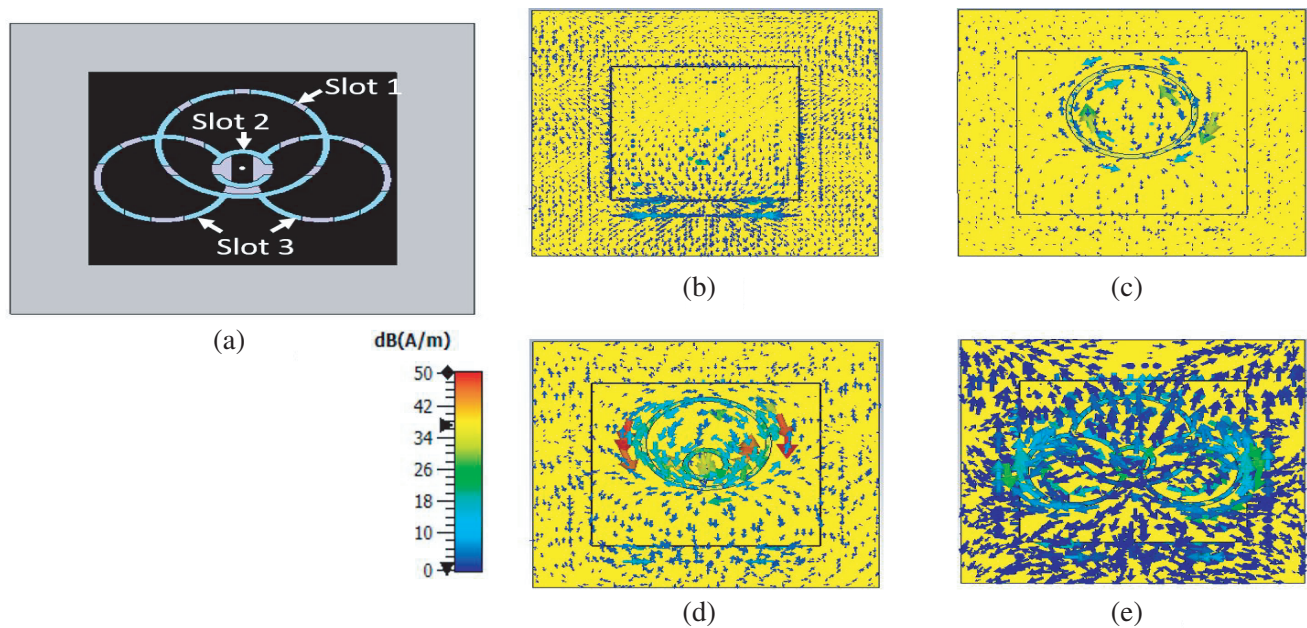


Figure 4. (a) Wide-band cavity antenna. (b) Surface currents of antenna without any slots. (c) With slot 1. (d) With slot 2. (e) With slot 3.

without changing the physical dimensions. This increased electrical length makes the cavity antenna to also resonate in lower frequencies. By appropriately designing the slots, the cavity antenna starts to resonate in multiple frequencies which increases the bandwidth of the antenna. The final configuration of the substrate placed at the top part of the cavity is shown in Fig. 3(b). This substrate is then covered with metal to complete the cavity.

The simulated impedance bandwidth for the antenna is 2.4 GHz (5.05 GHz–7.45 GHz) as shown in Fig. 5(a). The gain of the wide-band cavity antenna is shown in Fig. 5(b). The simulated bandwidth has increased from 7.3% for narrow-band to 40% for wide-band cavity antenna. The radiation pattern of the antenna is shown in Fig. 6. The half-power beamwidth (HPBW) is 96° , and the front-to-back ratio is 13 dB.

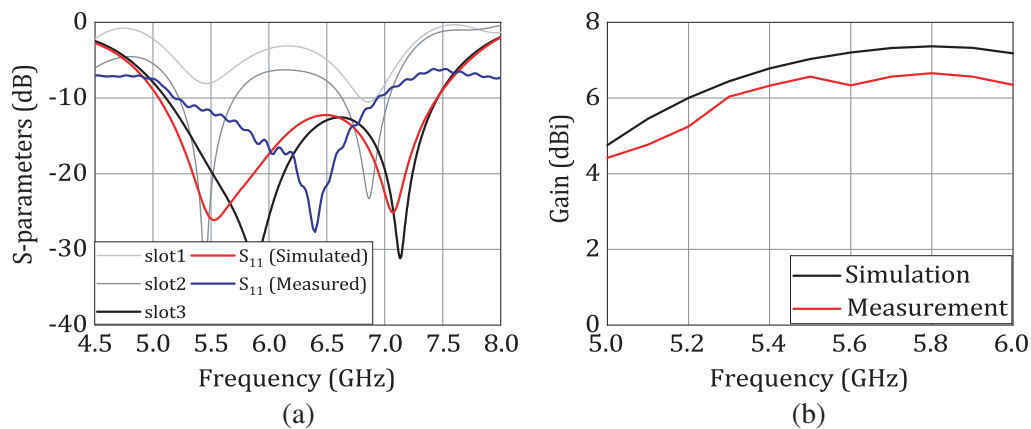


Figure 5. (a) Return-loss characteristics of wide-band cavity antenna. (b) Gain of wide-band cavity antenna.

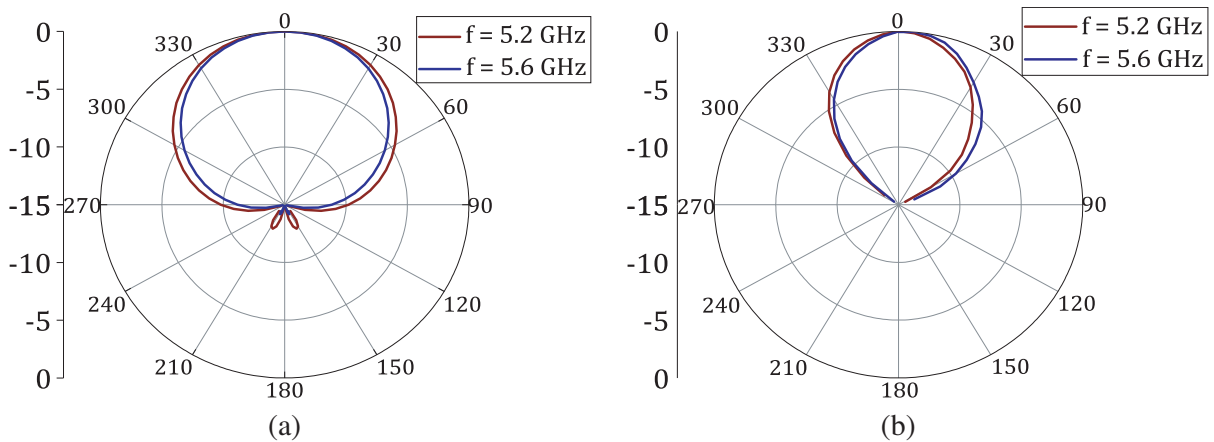


Figure 6. Radiation patterns at 5.2 GHz and 5.6 GHz. (a) Simulation. (b) Measurement.

2.3. Wide-Band Cavity Antenna with Slider

Now, the objective is to introduce a beam tilt in the designed wide-band cavity antenna. The beam tilt must also ensure that the scanning loss is minimum at the scanned angle, and the tilt is stable for a wide frequency range. The component of the antenna responsible for beam tilting is the slider that is designed and placed within the cavity of the antenna as shown in Fig. 7. The slider is designed using a PLA substrate with a thickness of 0.5 mm. It is then placed in the cavity space between the wall at the rear end of the cavity and the coaxial input pin as shown in Fig. 7(b). Initially, the slider shown in Fig. 7(c) is placed at the bottom of the cavity and then moved towards the top. For various heights of the slider from bottom to top, the beam tilt of the antenna increases from 0° to 20° . This tilt remains for frequencies from 5.2 GHz to 5.8 GHz or 10% of the bandwidth. Fig. 7(d) depicts the design evolution for the slider design. It was observed that a slider with a rectangular pattern imparts maximum beam tilt, and a slider design with a circular pattern imparts beam tilt for a wide frequency range. So combining the patterns to form an elliptical pattern results in maximum beam tilt for a wide frequency range.

The simulated impedance bandwidth for the antenna is 1.72 GHz (5.18 GHz–6.9 GHz) as shown

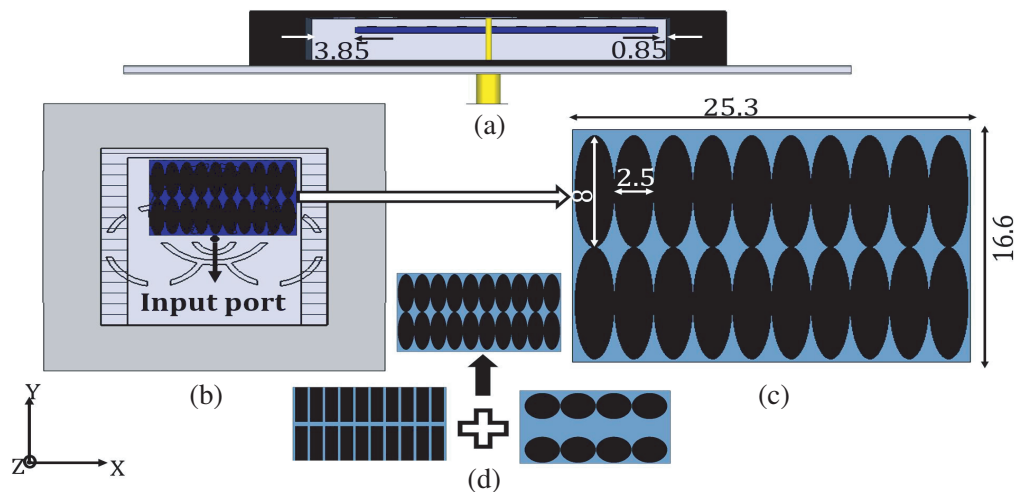


Figure 7. Schematic of wide-band cavity antenna with slider. (a) Front view. (b) Top view. (c) Top view of the slider. (d) Design evolution for the slider.

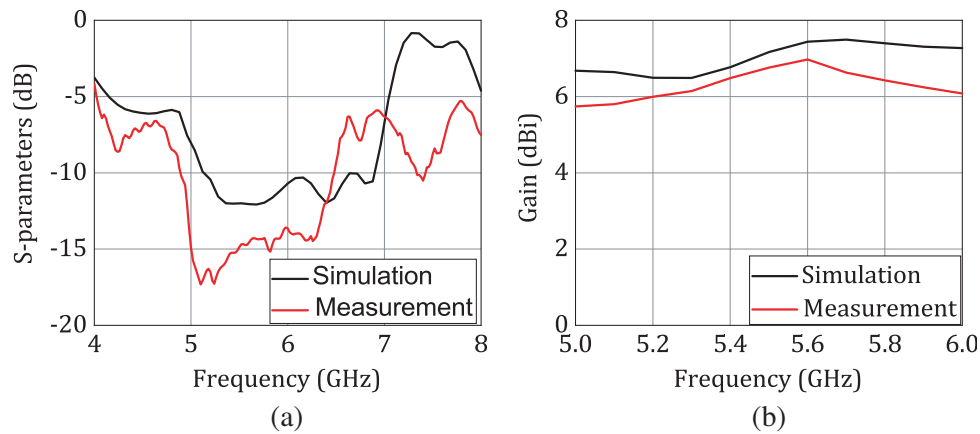


Figure 8. (a) Return-loss characteristics of wide-band cavity antenna with slider. (b) Gain of wide-band cavity antenna with slider.

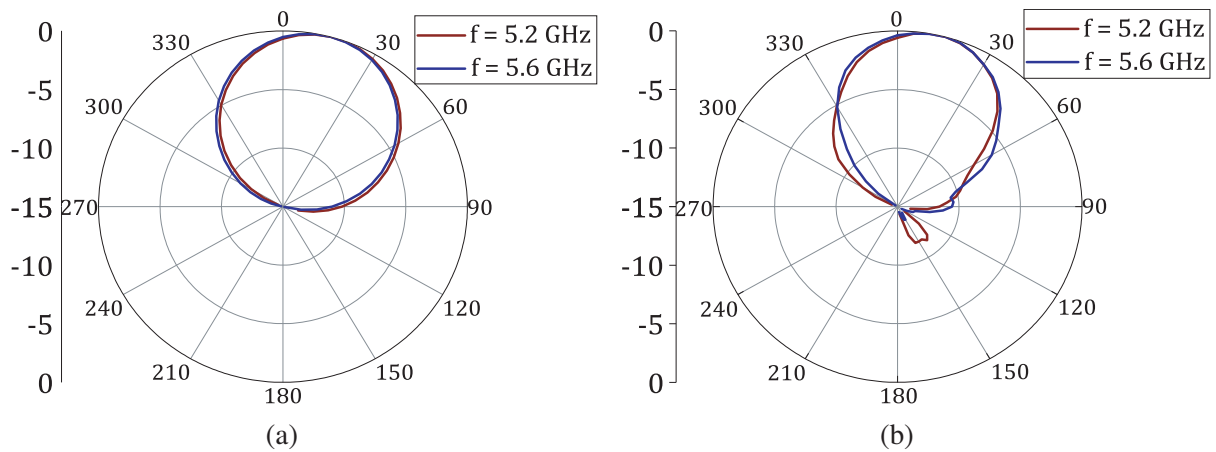


Figure 9. Radiation patterns at 5.2 GHz and 5.6 GHz. (a) Simulation. (b) Measurement.

in Fig. 8(a). The gain of the wide-band cavity antenna after the placement of the slider is shown in Fig. 8(b). The radiation patterns for the antenna for 5.2 GHz and 5.8 GHz are shown in Fig. 9. A similar tilted radiation pattern is maintained for all frequencies in this range. The half-power beamwidth (HPBW) of the antenna is 72° , and the front-to-back ratio is 17.5 dB.

2.3.1. Theoretical Analysis of the Slider

The slider inside the cavity influences the radiation pattern of the antenna resulting in a beam tilt. To better understand this phenomenon the slider was modeled as a dielectric block with a high dielectric constant. Fig. 10(a) shows the slider inside the cavity, and Fig. 10(b) shows the dielectric constant model inside the antenna cavity. This dielectric model has the same length and width as the slider, and the height is the same as the cavity height. As the slider moves inside the cavity air gap from bottom to top, the dielectric constant of the air cavity is affected. To verify this premise, the dielectric constant of the model was varied. It was observed that for dielectric constant variation from 1 to 4.39 the beam tilting of the antenna was comparable to the beam tilting that materialized while the slider moved from the bottom to the top of the cavity. The beam tilt of the antenna increases when the slider is moved from bottom to top inside the cavity. In the dielectric model of the slider, the beam tilt increases when the dielectric constant of the model is increased. The data are tabulated in Table 1.

The radiation patterns for both the sets are shown in Fig. 11 for beam tilting from 0° to 20° . As

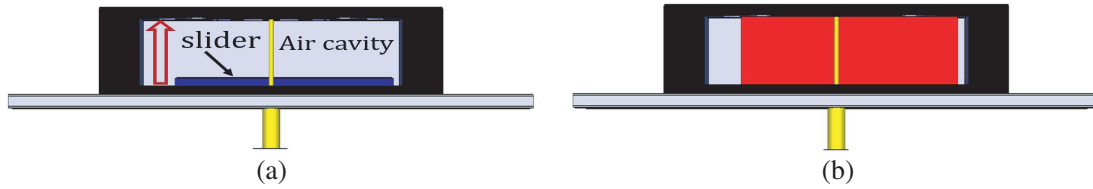


Figure 10. Wide-band cavity antenna with (a) slider, (b) varying dielectric block in the place of slider.

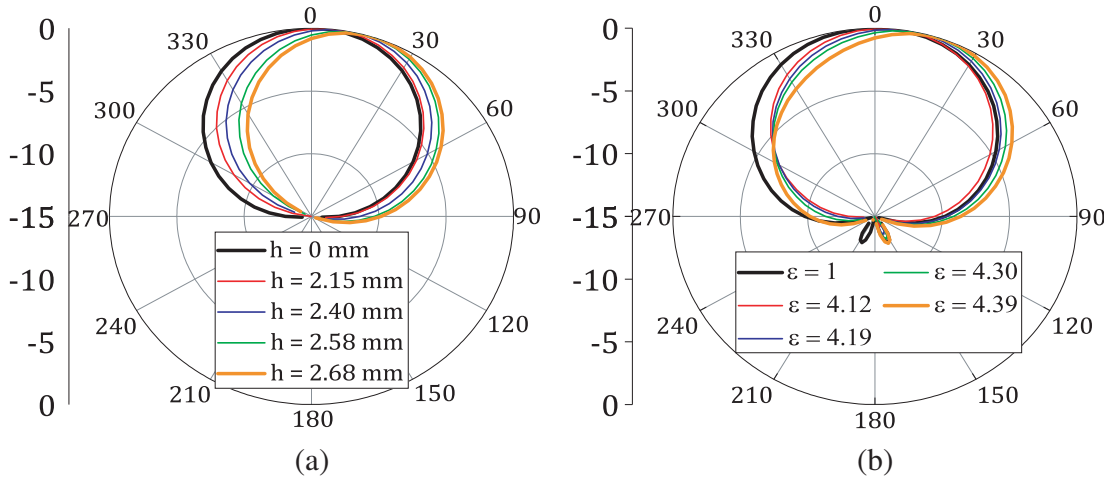


Figure 11. Radiation patterns at 5.2 GHz. (a) When height of the slider is varied across the cavity. (b) When the dielectric constant of the block is varied.

Table 1. Antenna beam tilt.

h	ϵ	beam tilt
0.00	1.00	0°
2.15	4.12	5°
2.40	4.19	10°
2.58	4.30	15°
2.68	4.39	20°

seen in Figs. 12(a)–(b) the E-field distribution along the mid-section of the antenna indicates the slider causing a field disturbance inside the cavity resulting in a deflected main beam. Figs. 12(c)–(d) shows the electric field distributions inside the cavity without and with the slider. For a cavity antenna, there is a uniform distribution of the electric field at both edges of the cavity making the antenna to radiate at the broadside. When the slider is introduced, there is a concentration of electric field towards the right edge of the antenna. As a consequence, the field intensity gets shifted which generates the tilted radiation beam.

2.4. Fabrication and Measurement

A prototype of the proposed antenna has been fabricated as shown in Fig. 13 to validate the simulation results. The cavity structure for the antenna is 3D printed. The 3D printing was performed using a Raise 3D RXP2200 3D printer a widely used commercial low-budget 3D printer. The lower part of the cavity antenna and ground plane is completed by pasting copper tape of 80 μ thickness. For the top

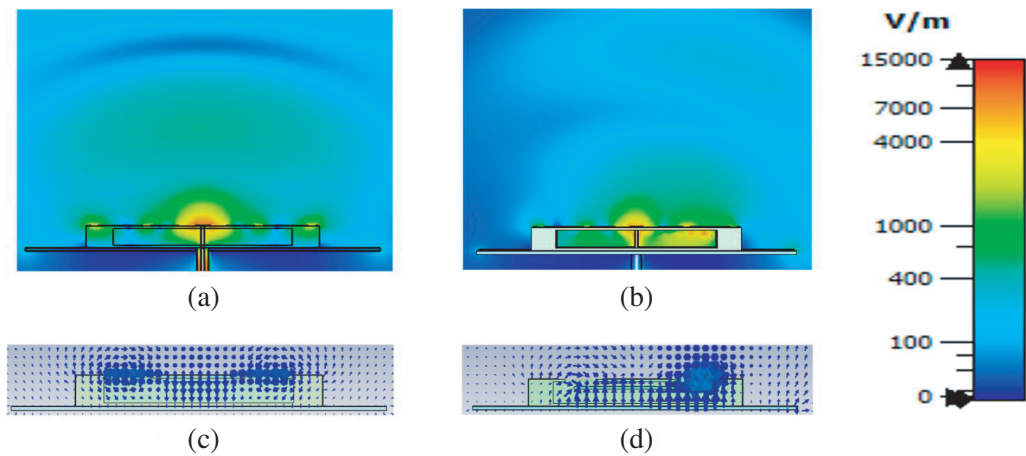


Figure 12. Electric-field of the cavity antenna. (a) Without slider. (b) With slider at 5.2 GHz.

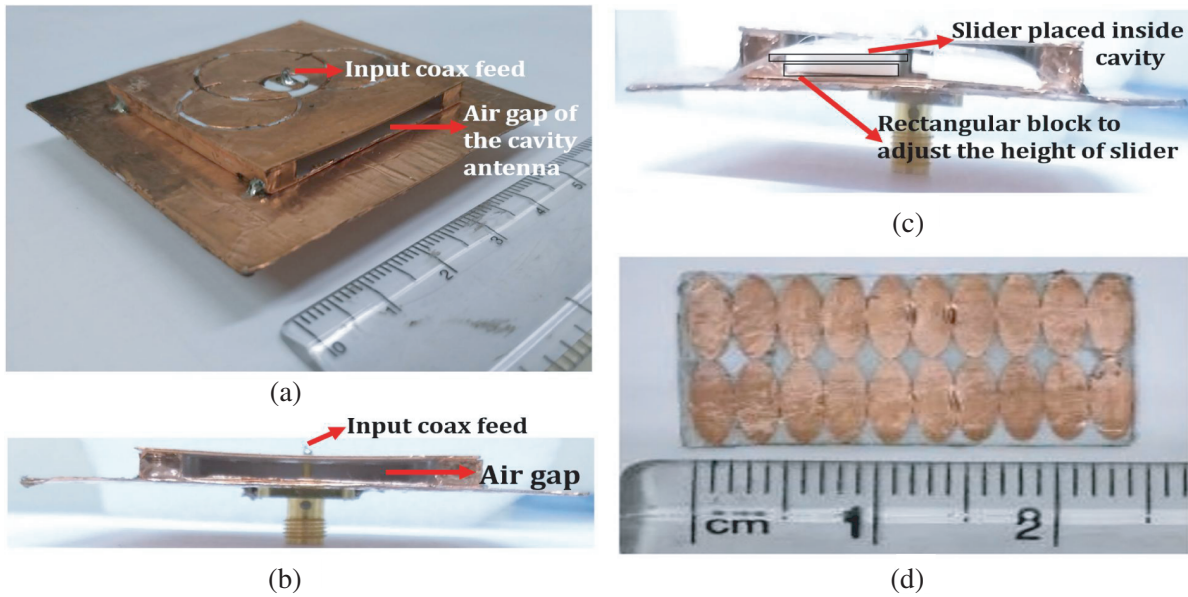


Figure 13. (a) Fabricated wide-band cavity antenna. (b) Side view. (c) Side view of the antenna after placing the slider. (d) Slider to be placed inside the antenna cavity.

part of the cavity, the copper was pasted, and the copper at the slots was removed by making proper incisions at slot positions. The slider design was fabricated by the photolithographic process. The slider is extended outside in order to assist in controlling the slider height from outside the cavity. 3-D printed blocks of required heights are then placed inside the cavity to keep the slider in position. The beam tilt is achieved from 0° to 20° by varying the height of the dielectric blocks that will keep the blocks at their required heights. Anritsu MS2028C VNA was used to measure the reflection coefficient of the antenna. The far-field measurements were conducted inside an anechoic chamber where ETS-Lindgreen 3115 Model double ridged waveguide horn antenna was used as the standard gain antenna for the measurement.

3. CAVITY ANTENNA ARRAY DESIGN

3.1. Two-Element Cavity Antenna Array

With the proposed element in Section 2 a linear two-element cavity antenna array is adopted as shown in Fig. 14. The array elements are arranged linearly on a ground plane of size $2.1\lambda \times 1.2\lambda$. The distance between the two elements is 1 mm, and the center-to-center distance between the elements is 0.8λ . The simulated impedance bandwidth for the antenna array is 2.43 GHz (5.07 GHz–7.5 GHz) as shown in Fig. 15(a), and the gain of the antenna array is shown in Fig. 15(b).

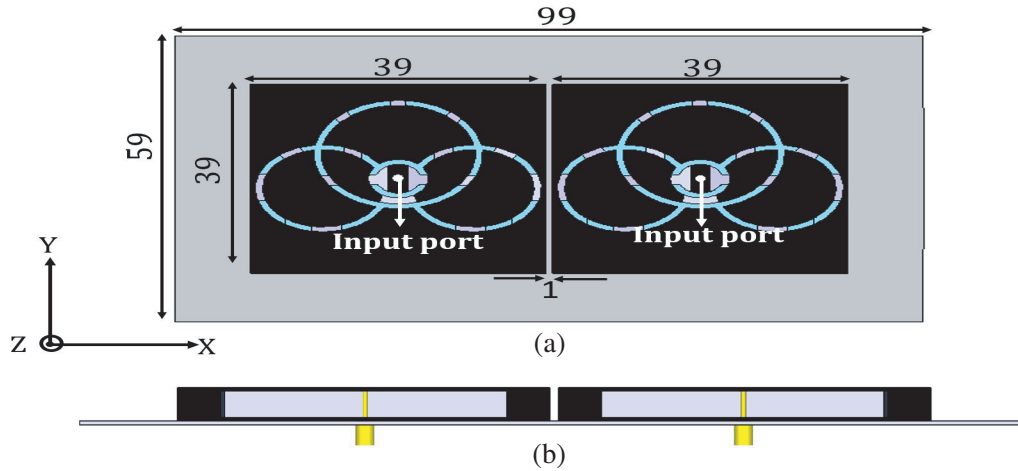


Figure 14. Schematic of two element cavity antenna array. (a) Top view. (b) Front view.

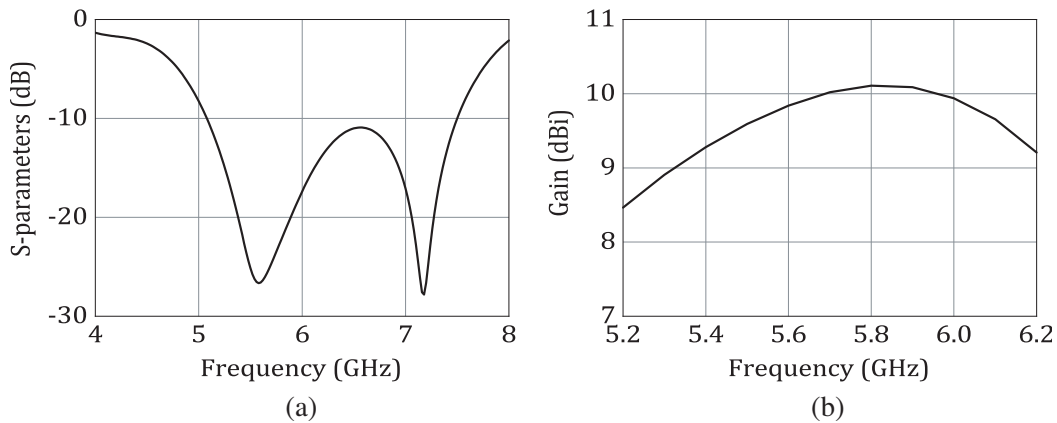


Figure 15. (a) Return-loss characteristics. (b) Gain of wide-band two-element antenna array.

3.2. Two-Element Cavity Slot Antenna Array with Slider

As shown in Fig. 16, in a two-element cavity array, the slider is placed inside the cavity of the antenna to the right. In this phase-shifter-less method of beam scanning, beam scanning occurs when the slider is moved from bottom to top inside the cavity. When the slider is placed in the right side cavity antenna and moved inside the cavity vertically the beam gets tilted towards $+20^\circ$. When the slider is placed in the left side cavity antenna and moved inside the cavity vertically the beam gets tilted towards -20° . By using two sliders in both cavity antennas the beam can be scanned from -20° to $+20^\circ$ by keeping the slider at required heights inside the cavity.

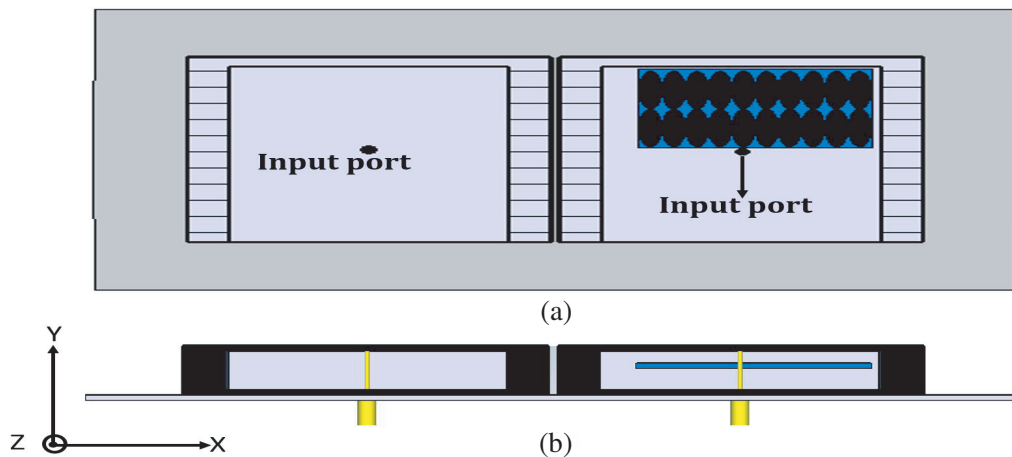


Figure 16. Schematic of two element cavity antenna array with slider. (a) Top view. (b) Front view.

The simulated impedance bandwidth for the antenna is 2.4 GHz (5.12 GHz–7.52 GHz) as shown in Fig. 17(a), and the gain of the antenna is 9.6 dB as shown in Fig. 17(b). The gain of the antenna in Fig. 17(b) is at 20° scanned angle. It is clear from the graph that for 20% fractional bandwidth the gain of the antenna varies from 9.6 dB to 9.3 dB limiting the scanning loss for wideband antenna within 0.3 dB. The radiation pattern for the two-element antenna array is shown in Fig. 18(a). The half-power beamwidth (HPBW) of the antenna is 33°, and the front-to-back ratio is 19 dB. The radiation pattern for the two-element antenna array with slider is shown in Fig. 18(b) where the beam-tilt for wide frequencies is visible. The half-power beamwidth (HPBW) of the antenna is 35°, and the front-to-back ratio of an antenna is 26 dB. The side lobe levels can be further reduced by increasing the ground plane dimensions. The electric field distributions of the array with and without the slider are shown in Fig. 19. The field shown in Fig. 19(b) is at 20° beam scanning of the antenna array when the slider is at 3.25 mm from the bottom of the antenna cavity.

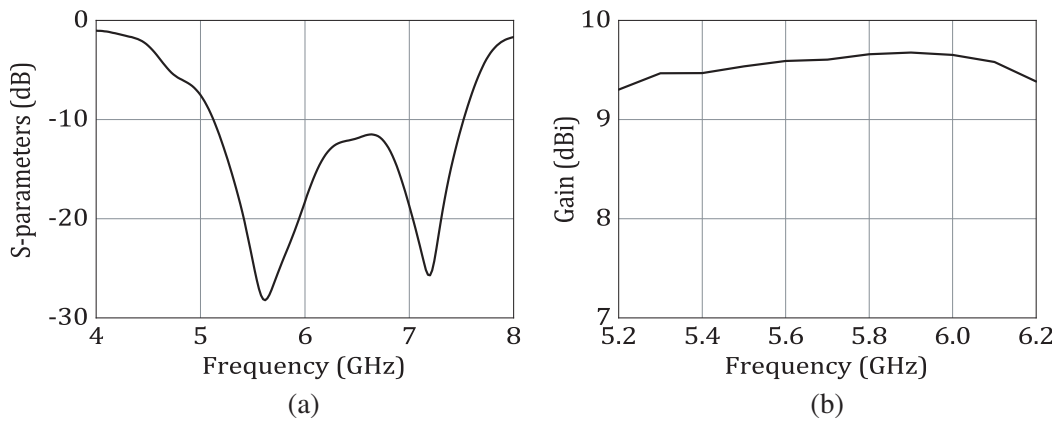


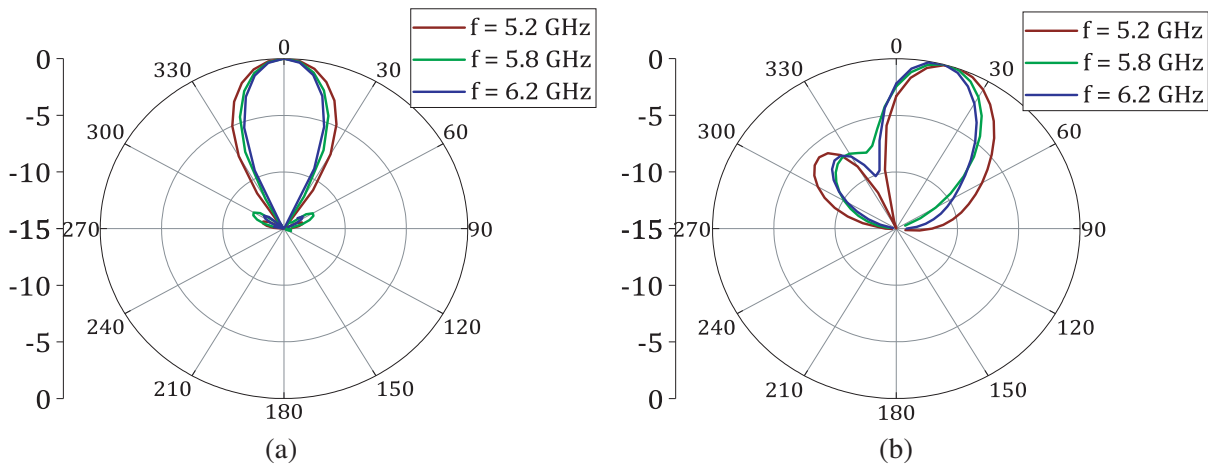
Figure 17. (a) Return-loss characteristics. (b) Gain of wide-band two-element antenna array with slider.

Comparisons of the bandwidth, scanning range, scanning loss along with the scanning technique of the proposed cavity antenna and some reported designs are described in Table 2. As observed from the table, the proposed design has only 0.3 dB scanning loss while scanning from broadside to 20° for a 20% fractional bandwidth. The frequency range of the proposed antenna considered is the range that yields the beam tilt. For the proposed antenna the beam tilt does not vary for a 20% fractional

Table 2. Comparison of the proposed antenna.

Ref.	[12]	[13]	[31]	[32]	[33]	PA
Frequency Range (GHz)	9.05–9.65	11	8.86–9.84	8–12	16–18	5–6.2
Fractional Bandwidth (%)	7	-	10.5	40	8.8	20
Size (λ)	$\lambda \times 9.7\lambda \times \lambda$	$6\lambda \times 6\lambda \times 0.5\lambda$	$5\lambda \times 1.2\lambda \times 0.5\lambda$	$3.23\lambda \times 3.1\lambda \times 0.27\lambda$	$5.6\lambda \times 1.6\lambda \times 8\lambda$	$2.1\lambda \times 1.2\lambda \times 0.1\lambda$
Scan Directions ($^\circ$)	36°	$\pm 51^\circ$	14°	$\pm 37^\circ$	$\pm 26^\circ$	$\pm 20^\circ$
Gain (dBi)	12.64	19.4	19.11	13.5	13.4	9.6
Gain variation through scan angle (dB)	1.3	3	0.8	2.1	1.5	0.8
Scanning loss through bandwidth (dB)	beam-tilt only at 9.35 GHz	beam-tilt only at 11 GHz	beam-tilt only at 9.35 GHz	Beam scanning varies within the frequency range	Beam scanning only at 17 GHz	0.3
Beam scanning technique	rotating dielectric slab inside wave-guide	rotation of the metasurface pair	rotating two dielectric slabs inside wave-guide	physically rotating antenna elements	insertion of tuning screws into waveguide	Varying the height of the slider inside the cavity
Radiation efficiency (%)	61	89	79	51	90	91

*PA = Proposed antenna

**Figure 18.** Simulated radiation patterns at 5.2 GHz, 5.8 GHz, 6.2 GHz. (a) Without slider. (b) With slider.

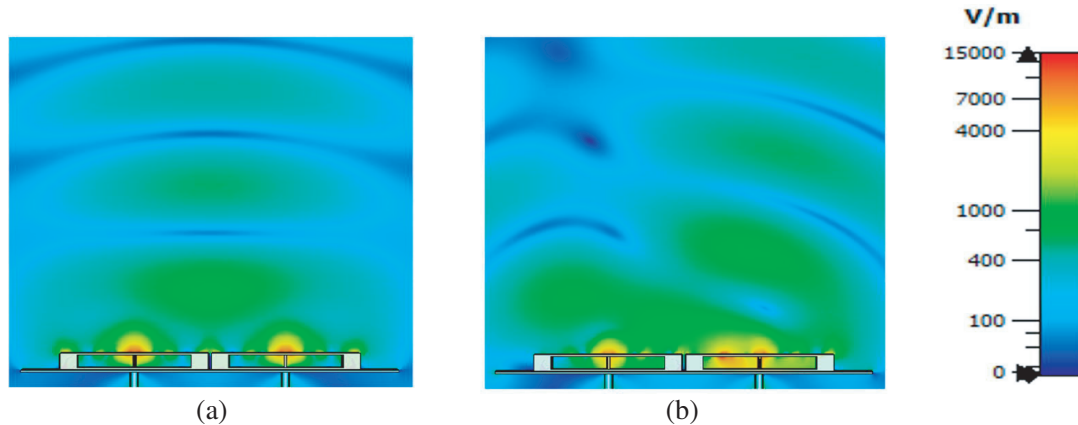


Figure 19. Electric-field distribution of two element array. (a) Without slider. (b) With slider.

bandwidth, and the beam is very stable at the scanned angle of 20° . From Table 2 it is evident that the previous studies have achieved beam tilt only at the design frequency, and the scan angle varies for different frequencies within the bandwidth. The proposed design has a high radiation efficiency of 91% resulting from the presence of air cavity and absence of any phase shifters and active devices. Hence, the proposed antenna shows great potential for directional wide-band antennas for WLAN applications.

4. CONCLUSION

Scanning loss reduction of a cavity antenna throughout the bandwidth as well as the scanned angle using a slider is presented. By shifting the slider from bottom to top inside the air cavity the beam is scanned from 0° to 20° . Considering the scanning range of the antenna, it has the ability to provide a total 3-dB coverage of 60° . The beam tilt of the antenna is sustained for 20% of antenna bandwidth with gain reduction of only 0.3 dB throughout the bandwidth. This bandwidth for which the beam tilt is sustained by the antenna is more than the reported bandwidth in the literature. Along with this high bandwidth, the gain variation while scanning the beam is also limited to only 0.8 dB. The proposed antenna thus ensures high signal strength for its 3-dB antenna beam width. Proper care must be taken to ensure that the appropriate slider height is maintained. The proposed design is validated for a single element antenna and for a two-element antenna array.

REFERENCES

1. Karmakar, R., S. Chattopadhyay, and S. Chakraborty, "Impact of IEEE 802.11n/ac phy/mac high throughput enhancements on transport and application protocols — A survey," *IEEE Communications Surveys Tutorials*, Vol. 19, No. 4, 2050–2091, 2017.
2. Rocca, P., G. Oliveri, R. J. Mailloux, and A. Massa, "Unconventional phased array architectures and design methodologies — A review," *Proceedings of the IEEE*, Vol. 104, No. 3, 544–560, 2016.
3. Hansen, R. C., *Phased Array Antennas*, 2nd Edition, Wiley, 2009.
4. Rao, S. K. and C. Ostroot, "Design principles and guidelines for phased array and reflector antennas [antenna applications corner]," *IEEE Antennas and Propagation Magazine*, Vol. 62, No. 2, 74–81, 2020.
5. Chandran, A. R., S. Morris, S. Raman, N. Timmons, and J. Morrison, "Microstrip patch based switched beam antenna at 2.45 GHz for wireless sensor network applications," *Journal of Electromagnetic Waves and Applications*, Vol. 31, No. 13, 1333–1341, 2017.
6. Tian, H., L. J. Jiang, and T. Itoh, "A compact single-element pattern reconfigurable antenna with wide-angle scanning tuned by a single varactor," *Progress In Electromagnetics Research C*, Vol. 92, 137–150, 2019.

7. Razmjoo, H., H. Abiri, and A. Yahaghi, "A novel dual band patch design for electrical steerable reflectarray antennas," *Journal of Electromagnetic Waves and Applications*, Vol. 34, No. 1, 35–50, 2020.
8. Yang, J., S.-S. Qi, W. Wu, and D.-G. Fang, "A novel high-gain sum and difference conical beam-scanning reflector antenna," *IEEE Access*, Vol. 8, 103 291–103 300, 2020.
9. Ramazannia Tuloti, S. H., P. Rezaei, and F. Tavakkol Hamedani, "High-efficient wideband transmitarray antenna," *IEEE Antennas and Wireless Propagation Letters*, Vol. 17, No. 5, 817–820, 2018.
10. Nguyen, B. D. and S. V. Tran, "Beam-steering reflectarray based on two-bit aperture-coupled reflectarray element," *Journal of Electromagnetic Waves and Applications*, Vol. 32, No. 1, 54–66, 2018.
11. Wang, H.-F., Z.-B. Wang, Z.-H. Wu, and Y.-R. Zhang, "Beam-scanning lens antenna based on elliptical paraboloid phase distribution metasurfaces," *IEEE Antennas and Wireless Propagation Letters*, Vol. 18, No. 8, 1562–1566, 2019.
12. Ghasemi, A. and J.-J. Laurin, "Beam steering in narrow-wall slotted ridge waveguide antenna using a rotating dielectric slab," *IEEE Antennas and Wireless Propagation Letters*, Vol. 17, No. 10, 1773–1777, 2018.
13. Afzal, M. U. and K. P. Esselle, "Steering the beam of medium-to-high gain antennas using nearfield phase transformation," *IEEE Transactions on Antennas and Propagation*, Vol. 65, No. 4, 1680–1690, 2017.
14. Bjorgaard, J., M. Hoyack, E. Huber, M. Mirzaee, Y.-H. Chang, and S. Noghianian, "Design and fabrication of antennas using 3D printing," *Progress In Electromagnetics Research C*, Vol. 84, 119–134, 2018.
15. McKerricher, G., D. Titterington, and A. Shamim, "A fully inkjet-printed 3-D honeycomb-inspired patch antenna," *IEEE Antennas and Wireless Propagation Letters*, Vol. 15, 544–547, 2016.
16. Whittow, W. G., S. S. Bukhari, L. A. Jones, and I. L. Morrow, "Applications and future prospects for microstrip antennas using heterogeneous and complex 3-D geometry substrates," *Progress In Electromagnetics Research*, Vol. 144, 271–280, 2014.
17. Lou, Q., R.-X. Wu, and Y. Tian, "A rectangular loop yagi-uda antenna by the two materials 3-D printing technology," *IEEE Antennas and Wireless Propagation Letters*, Vol. 17, No. 11, 2017–2020, 2018.
18. Shin, S.-H., D. F. Alyasiri, M. D'Auria, W. J. Otter, C. W. Myant, D. Stokes, Z. Tian, N. M. Ridler, and S. Lucyszyn, "Polymer-based 3-D printed ku-band steerable phased-array antenna subsystem," *IEEE Access*, Vol. 7, 106 662–106 673, 2019.
19. Singh, D., A. Jain, and R. P. Yadav, "Development of circular loop frequency selective surface using 3-D printing technique," *Progress In Electromagnetics Research M*, Vol. 90, 195–203, 2020.
20. He, Y., W. Tian, and L. Zhang, "A novel dual-broadband dual-polarized electrical downtilt base station antenna for 2G/3G applications," *IEEE Access*, Vol. 5, 15 241–15 249, 2017.
21. Izzat, N. M. K. M., M. L. Zimmerman, and K. E. Linehan, "Antenna, base station and power coupler," U.S. Patent 6,922,169 B2, July 26, 2005.
22. Luk, K.-M. and Z. N. Chen, *Antennas for base stations in Wireless Communications*, 3rd Edition, McGraw Hill, 2009.
23. Zhang, H. and Y.-Z. Yin, "Single-layer single-feed wideband omnidirectional microstrip antenna with rotating square patches," *Progress In Electromagnetics Research Letters*, Vol. 93, 27–34, 2020.
24. Roy, S., K. L. Baishnab, and U. Chakraborty, "Beam focusing compact wideband antenna loaded with mu-negative metamaterial for wireless lan application," *Progress In Electromagnetics Research Letters*, Vol. 83, 33–44, 2018.
25. Ghaemi, K. and N. Behdad, "A low-profile, wideband antenna with vertically polarized directional radiation," *IEEE Antennas and Wireless Propagation Letters*, Vol. 15, 1093–1096, 2016.

26. Martinis, M., L. Bernard, K. Mahdjoubi, R. Sauleau, and S. Collardey, "Wideband antenna in cavity based on metasurfaces," *IEEE Antennas and Wireless Propagation Letters*, Vol. 15, 1053–1056, 2016.
27. Sánchez Hernández, D., *Multiband Integrated Antennas for 4G Terminals*, Artech House Inc, January 2008.
28. Tayli, D. and M. Gustafsson, "Physical bounds for antennas above a ground plane," *IEEE Antennas and Wireless Propagation Letters*, Vol. 15, 1281–1284, 2016.
29. Garg, R., P. Bhartia, I. Bahl, and A. Ittipiboon, *Microstrip Antenna Design Handbook*, 1st Edition, Artech House, Inc., USA, 2001.
30. Ludvig-Osipov, A., J.-M. Hannula, P. Naccachian, and B. L. G. Jonsson, "Physical limitations of phased array antennas," *IEEE Transactions on Antennas and Propagation*, Vol. 69, No. 9, 5512–5523, 2021.
31. Ghasemi, A. and J.-J. Laurin, "A continuous beam steering slotted waveguide antenna using rotating dielectric slabs," *IEEE Transactions on Antennas and Propagation*, Vol. 67, No. 10, 6362–6370, 2019.
32. Yao, Y.-L., F.-S. Zhang, and F. Zhang, "A new approach to design circularly polarized beam-steering antenna arrays without phase shift circuits," *IEEE Transactions on Antennas and Propagation*, Vol. 66, No. 5, 2354–2364, 2018.
33. Sanchez-Olivares, P., J. L. Masa-Campos, A. T. Muriel-Barrado, R. Villena-Medina, and G. M. Fernandez-Romero, "Mechanically reconfigurable linear array antenna fed by a tunable corporate waveguide network with tuning screws," *IEEE Antennas and Wireless Propagation Letters*, Vol. 17, No. 8, 1430–1434, 2018.